Analysis of the response of a roadway bridge under extreme flooding-related events: Scour and debris-loading

M. Kosič [a],[*], L.J. Prendergast [b], A. Anžlin [a]

[a] *Section for Bridges and Engineering Structures, Department for Structures, Slovenian National Building and Civil Engineering Institute (ZAG), Dimičeva ulica 12, Ljubljana, Slovenia*
[b] *Department of Civil Engineering, Faculty of Engineering, University of Nottingham, Nottingham, NG7 2RD, United Kingdom*

A R T I C L E   I N F O

A B S T R A C T

Hydraulic actions on bridges are a leading cause of failure, especially due to the occurrence of scour erosion. Due to climate change, flooding and scour risks are exacerbating for bridges worldwide, leading to a significant stress burden on asset management agencies. Assessing structures for scour has received significant attention in recent years, however, there are few studies which investigate the influence of scour on the components of a bridge to understand how various elements interact. Moreover, the presence of debris loading, which can occur due to flooding causing debris to become lodged at structures, has not received significant attention. Debris can worsen scour conditions and increase hydraulic loading on a bridge. In this paper, an analysis of the response of various components of a roadway bridge when exposed to extreme flooding is conducted. The influence of scour and debris on hydraulic loading, internal forces, modal periods, and utilization ratios of various bridge components is ascertained. A numerical model is developed using OpenSees employing two different methods to model the soil-structure interaction. Results for several flooding scenarios show how the various bridge elements are influenced by variations in water height and velocity, scour depth, and presence of debris.

1. Introduction

Global mean temperatures are rising, which is resulting in increased frequency of both drought and floods worldwide [1]. While significant efforts are being made by governments to maintain global mean temperatures below a 1.5 °C increase [2], it must nevertheless be recognised that bridges and other critical infrastructure need to be resilient against more frequent extreme weather events. In tandem with climate-related additional stresses being placed on infrastructure, many bridges are approaching or have exceeded their original design lives, placing a significant burden on asset managers. This issue requires that bridge owners not only maintain the assets according to currently accepted bridge management principles [3], but also use novel approaches for performing reliability analyses on existing bridges exposed to constantly changing hazards.

Increased frequency of flooding poses risks to bridges through larger hydraulic loading; as well as higher risks of scour erosion, which is the term given to the action of water washing away soil from around foundations [4]. This is already one of the leading causes of bridge failure worldwide [5–8]. One early study suggested that of five hundred

bridge failures occurring between 1989 and 2000 in the United States, 53% were caused by flooding and scour-related issues [7]. Scour occurs in three main forms; general scour due to natural riverbed changes over time [9], contraction scour due to narrow bridge openings [10], and local scour due to the presence of obstacles such as bridge foundations obstructing flow [4,11,12]. When combined, scour can significantly lower the elevation of the riverbed relative to installed structures (primary damage), which influences the stiffness and capacity of bridge foundations [13–17], and can lead to serviceability problems such as differential settlement, or partial and total collapse (secondary damage) [5,18]. Scour is exacerbated during flooding conditions, and scour depths can be further increased as a result of debris becoming trapped at bridge openings [19]. The specific effects of scour on bridges have been investigated by several authors. For example, Klinga and Alipour [20] investigated the effects of extreme scour on the static and dynamic response characteristics of piled bridges, and concluded that scour reduces lateral stiffness, increasing modal periods. Tubaldi et al. [21] developed a modelling strategy for multi-span masonry bridges subjected to scour, which can be used to evaluate the vulnerability under various flooding scenarios. Foti and Sabia [22] investigated the effect of scour on the modal properties and dynamic behaviour of a multi-span

* Corresponding author.
  E-mail address: mirko.kosic@zag.si (M. Kosič).

Nomenclature

a	Pier width
a_d^*	Equivalent pier width
A_b	Area of the foundation base
A_d	Projected wetted area in the direction of the flow
A_l	Projected wetted area in the direction perpendicular to the flow
$\overline{A_s}$	Normalised resistance factor
c	Cohesion of the soil
c'	Effective cohesion of the soil
C_d	Hydrodynamic drag coefficient
C_l	Hydrodynamic lift coefficient
d_c	Depth correction factor, according to Meyerhof (1963)
d_q	Depth correction factor, according to Meyerhof (1963)
d_γ	Depth correction factor, according to Meyerhof (1963)
d_{sp}	Wetted depth of deck
d_{ss}	Wetted depth of the solid superstructure
d_{wgs}	Distance from the deck soffit to flood water surface
D_f	Diameter of the foundation
D_E	Embedment depth of the foundation
D_r	Relative density
E	Elastic modulus of the soil
F_d	Hydrodynamic drag force
F_l	Hydrodynamic lift force
F_r	Froude number
g	Acceleration of gravity
G	Shear modulus of the soil
H	Water height
H_b	Foundation base horizontal force
H_{ub}	Foundation base ultimate sliding resistance
k	coefficient of subgrade reaction of the p-y springs
K	Coefficient of lateral earth pressure
K_{d1}	Debris shape coefficient
K_{d2}	Debris shape coefficient
K_{hb}	Foundation base initial horizontal stiffness
K_H^0	Horizontal stiffness of surface foundation
K_H^e	Horizontal stiffness of embedded foundation
K_V^0	Vertical stiffness of surface foundation
K_V^e	Vertical stiffness of embedded foundation
K_R^0	Rocking stiffness of surface foundation
K_R^e	Rocking stiffness of embedded foundation
K_T^0	Torsional stiffness of surface foundation
K_T^e	Torsional stiffness of embedded foundation
$K_{\varphi b}$	Initial rotational stiffness of the base of the foundation
K_1	Correction factor for pier nose shape in HEC-18 scour equation
K_2	Correction factor for angle of attack of the flow in HEC-18 scour equation
K_3	Correction factor for riverbed conditions in HEC-18 scour equation

L_f	Depth of the foundation
L_d	Length of the debris raft upstream from the pier face
M_b	Foundation base moment
M_{ub}	Foundation base ultimate moment
N_c	Soil bearing factor according to Meyerhof (1963)
N_q	Soil bearing factor according to Meyerhof (1963)
N_γ	Soil bearing factor according to Meyerhof (1963)
$(N_1)_{60}$	Overburden-corrected number of Standard Penetration Test (SPT) blows of the soil
N_{60}	Equivalent number of Standard Penetration Test (SPT) blows of the soil
$\overline{N}_{60}$	Average value of N_{60} blows of the soil in the influence zone of the foundation
P_r	Proximity ratio
p_u	Ultimate soil resistance per unit length
P_u	Ultimate force of p-y spring
q_c	CPT tip resistance
$q_{net,50}$	Net overburden pressure at 50% of foundation capacity
Q	Applied vertical load on the foundation base
Q_u	Ultimate force of q-z spring
R_f	Radius of the foundation
S_r	Relative submergence of the deck
$T_{1,x}$	First modal period in x- (traffic) direction
$T_{1,y}$	First modal period in y- (flow) direction
T_d	Thickness of the debris raft
T_u	Ultimate force of t-z spring
u_b	Foundation base horizontal displacement
u_{pb}	Foundation base displacement at the mobilisation of ultimate sliding resistance
v	Mean flow velocity
W_d	Width of the debris raft normal to the flow
y_{gs}	Vertical average distance from the deck soffit to the riverbed
y_s	Local scour depth
y_{50}	Displacements at 50% of the ultimate force of the p-y spring
z	Depth of the spring
z_{qz50}	Displacements at 50% of the ultimate force of the q-z spring
z_{tz50}	Displacements at 50% of the ultimate force of the t-z spring
Δz	Vertical spacing between p-y, t-z and q-z springs (tributary length)
φ'	Angle of friction of the soil
φ_b	Foundation base rotation
γ	Soil unit weight
γ'	Soil effective unit weight
δ	Friction angle of the soil-foundation interface
θ	Angle of attack of the flow in relation to the bridge pier
θ_{pb}	Rotation at full mobilisation of the spring
ν	Poisson's ratio
σ_v'	Vertical effective stress

bridge in Turin, Italy, and concluded that scour resulted in the asymmetric dynamic behaviour of the foundation.

Scour is very difficult to detect, and most asset management agencies still rely on visual inspections, which require divers to manually inspect foundations using crude scour depth-measuring instrumentation. These types of inspection tend to be costly, time-intensive, and subjective (based on diver judgement). This has been the impetus for the development of novel approaches to scour detection using installed scour sensors such as float-out devices [23,24], radar and sound pulse devices [9,25–28], sensors on driven rods [29,30], and electrical conductivity devices [28]. More recently, the focus has shifted to vibration-based damage detection approaches to identify scour using the response of the affected structures, by monitoring natural frequencies [15,31–36], mode shapes (and curvature) [14,16,37], as well as various other dynamic parameters [16,22]. This is arguably more informative as it directly assesses the impact a scour hole has on the affected structure, as opposed to simply measuring the depth of scour.

While monitoring bridges for scour is gaining traction, the decision to install health monitoring systems and sensors on affected structures must be balanced by the financial benefit of doing so, which can be

assessed using methods such as the value of information from Bayesian decision analysis [38,39]. In general, it will not be possible to install sensor systems on every bridge on a given network due to the often constrained budgets of asset management agencies. Alternative approaches are also required to facilitate assessing the risk posed by scour and hydraulic actions on bridges. In this paper, an analysis to identify the response of various components of a bridge when exposed to extreme flooding-related events is conducted. A numerical model of a bridge, a case study inspired by a road bridge in Croatia, is used to assess the impact of various flood-related damaging actions, including adverse hydraulic loads and debris-accumulation. The results show that, by processing collected information on the performance of the structure under various hydraulic scenarios, additional support for future decisions to increase the bridge resilience can be provided.

2. Description of the bridge

The bridge used as the inspiration for the model is a steel-riveted girder bridge that spans the Kupa River in central Croatia. It was constructed between 1945 and 1947 (Fig. 1) as a replacement for an older bridge built in 1889, which was demolished during World War II. The geometry, geotechnical conditions, hydrological data, and modal information, are described in the following sub-sections.

2.1. Geometry and materials

The material and geometrical data is described herein, as available from relevant as-built construction information. Some data was estimated from a retrofitting project conducted in 2017 along with a drone and bathymetric survey. The bridge has two main spans of length 48.6 m

with a central pier founded in the riverbed of the Kupa River. The total length of the bridge is 97.2 m, and its width is 12.4 m. It supports two traffic lanes and a pedestrian zone, which is constructed on cantilever beams at the upstream part of the bridge. The cross-section of the bridge is shown schematically in Fig. 2.

The two main girders have riveted I-shaped cross sections with changing thickness of the flanges to follow the bending moment line. The main girders are joined together every 4.05 m by riveted transverse beams, which are connected with seven I-shaped stringers that support the reinforced concrete (RC) slab of the deck (Fig. 2). At the abutments, the main girders are supported by longitudinal roller bearings with diameters 0.20 m (Fig. 1d). The transverse displacement of each bearing is restrained with shear keys of dimension 0.03 m × 0.06 m. At the central pier, the translation of the bridge is restrained in all directions by the use of shear pins of diameter 0.05 m. The pier and the abutments are made of reinforced concrete and are covered with stone cladding. Due to an unavailability of as-built construction plans, the depth of each foundation is assumed to be equal to that used for the original bridge from 1889 (equating to 5.8 m), for which partial historic construction plans were obtained from archives. The depth of the stone cladding was estimated to be equal to 0.15 m.

The mechanical characteristics of the superstructure were obtained from destructive testing performed during a retrofitting project for the structure. The steel grade for the superstructure was estimated to be equivalent to S235 according to EN-1993 [40], whereas the concrete grade of the bridge deck was estimated to be equivalent to C25/30 according to EN-1992–1 [41]. No data for the material characteristics of the bridge pier and foundations were available, therefore the quality of the concrete used was assumed equal to that used for the bridge deck (C25/30).
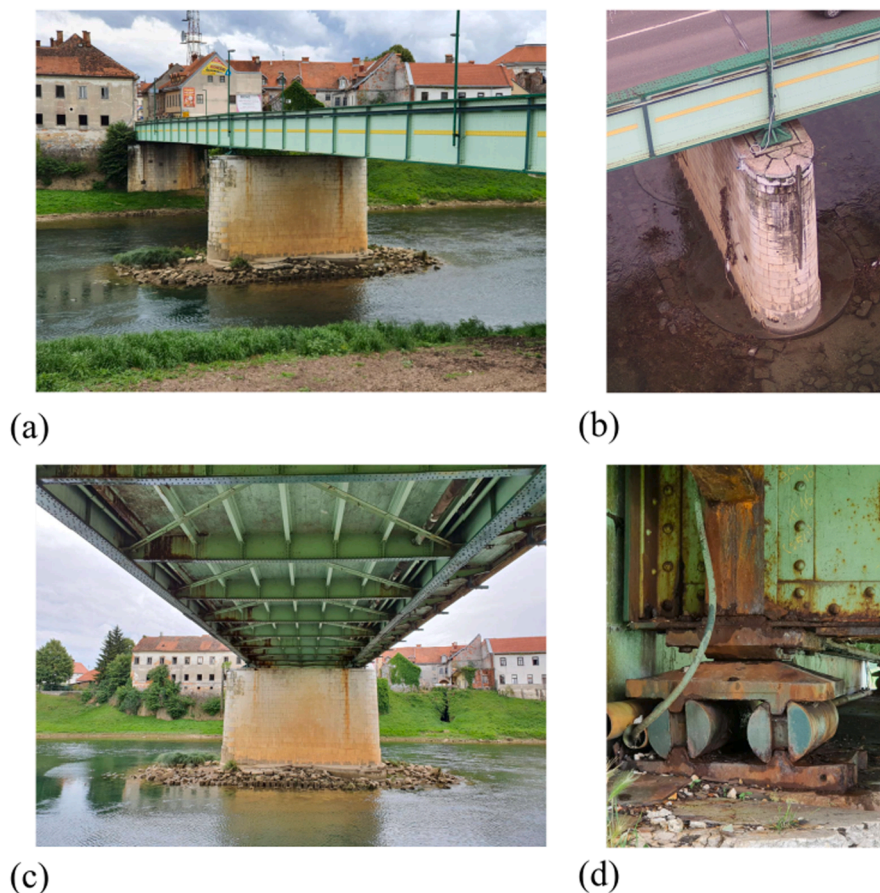

Fig. 1. Overview of the bridge geometry: (a) Side view, (b) Detail of the middle pier and well foundations, (c) View below the bridge deck, (d) Detail of the roller bearing at the abutment.
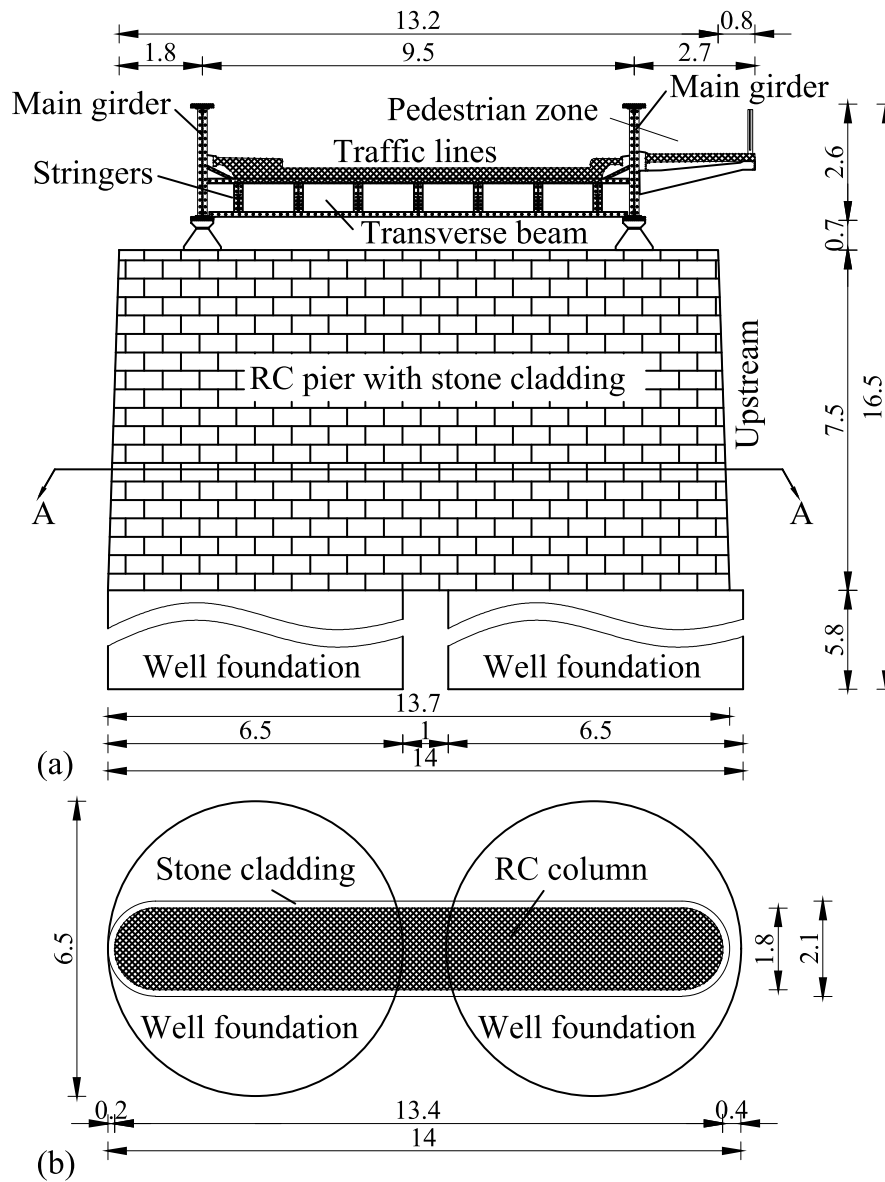
Fig. 2. (a) Cross-section of the modelled bridge in the first span, (b) Section A-A at the base of the pier.

2.2. Geotechnical data

The geotechnical characteristics at the site were defined from a nearby Cone Penetration Test (CPT) investigation, which was performed from the level of the abutment [42]. The CPT tip resistance, q_c, profile varies from an average of 10 MPa near surface, reducing to 1–2 MPa from approximately 1.5 m below ground level (bgl) to 6.5 m bgl, increasing to an average of 5 MPa between 6.5 m and 9 m bgl, increasing to > 10 MPa at greater depths. The soil profile was identified to be clay over the top 6 m, with sand extending to larger depths. Investigations performed directly near the foundation of the central pier were not available, however, the same stratigraphy was confirmed based on results of geophysics investigations. Energy-corrected Standard Penetration Test (SPT) blows (N_{60}) of 35 are achieved at the level of the foundation, revealing a soil Elastic modulus (E) of 100 MPa. The soil characteristics were modified to consider the influence of reduced overburden stresses at the foundation level of the central pier resulting from the soil being at a lower stress-state (because the location where the testing is conducted is at a different elevation). The reduction in the soil stiffness due to the reduced overburden was estimated according to the approach in Janbu [43], as referenced in Ref. [44]. This resulted in

the elastic modulus, shear modulus (G) and equivalent number of Standard Penetration Test (SPT) blows (N_{60}) being lower than those obtained (at the same depth) at the abutment. The overburden-corrected number of SPT blows of the sand layer amount to $(N_1)_{60} = 25$. Using empirical SPT correlations, the angle of friction is derived as 40° and the relative density, D_r, is 0.6. The dry unit weight of the soil, established from a borehole, is 19.8 kN/m³. The E under reduced overburden is 50 MPa, and G is 19 MPa, where the Poisson ratio is 0.3.

Table 1
Soil characteristics for modelling of soil-structure interaction at the middle pier.

Parameter	Value
Angle of friction (φ')	40°
Effective cohesion (c')	0 kPa
Soil unit weight (γ)	19.8 kN/m³
Poisson's ratio (ν)	0.30
Elastic modulus (E)	50 MPa
Shear modulus (G)	19 MPa
Equivalent SPT blows (N_{60})	19

The considered soil characteristics for modelling the Soil-Structure Interaction (SSI) at the central pier are summarized in Table 1.

2.3. Hydrological data

The hydrological data at the bridge was obtained from the Karlovac measuring station, located 20 m upstream of the bridge. Flood intensity was defined using measured water height (H) and mean flow velocity (v). The hydrological conditions at the measuring station are rather complex, as the stream stage-discharge curve (rating curve) exhibits hysteretic behaviour (Fig. 3), which indicate a non-stationary flow due to the influence of nearby effluents. The relationship between H and v is thus not uniquely defined. An estimation of the relation between the parameters was obtained from numerical simulations [45], which were conducted for three historical flood events from the years 2005, 2014 and 2015 (Fig. 3). In this study, the results of the simulations were idealized considering three flow velocity scenarios; a lower-bound of 0.5 m/s, a best estimate of 0.85 m/s, and an upper-bound of 1.2 m/s, as shown in Fig. 3.

2.4. Ambient vibration data

An ambient vibration survey conducted on the bridge enabled modal parameters to be determined [46]. Twelve tri-axial accelerometers were placed on the bridge, and the measurements were analysed using operational modal analysis, which allowed the identification of seven vibration modes of the bridge deck (4 translational and 3 torsional modes). The results were used for evaluation of the employed modelling approach (described subsequently) in the small-strain region. It was only possible to determine vibration modes of the bridge deck from the measurements, therefore, the obtained results are not suited for evaluation of the global bridge response, which is also influenced by SSI. This means a direct validation of the SSI modelling is not possible. An attempt to perform a lateral modal analysis with the use of two long-stroke shakers exciting the bridge in the horizontal direction proved unsuccessful due to large stiffness of the pier and insufficient capacity of the shakers. The modal frequencies of the bridge deck obtained from ambient vibration measurements are summarized in Table 2. These frequencies are used to validate the developed superstructure models. A comparison of mode shapes is omitted from the paper due to the inability to excite the lateral modes.

3. Modelling approach

A numerical model of the roadway bridge is developed, the various

Table 2
Ambient vibration data of the bridge deck obtained from the operational modal analysis.

Deck vibration mode	Frequency [Hz]	Period [s]
1st vertical	1.46	0.68
2nd vertical	2.32	0.43
1st transverse	4.76	0.21
3rd vertical	5.13	0.19

components of which are discussed in this section. The model is created using open-source finite-element software framework OpenSees [47,48]. Two modelling approaches are implemented with respect to simulation of SSI, elaborated below, resulting in two separate numerical models being used for the analysis of the bridge. As OpenSees does not provide a user-friendly graphical interface, a preliminary numerical model of the bridge was developed in CSI SAP2000 [49]. This model was then imported into OpenSeesPy [47] via a set of user-defined functions and enhanced to model SSI using the two approaches. A schematic showing both models is shown in Fig. 4.

3.1. Structural modelling

The bridge superstructure and foundations were modelled using linear elastic Timoshenko beam-column elements [50]. The schematic, loading, and boundary conditions are shown in Fig. 4. The bridge deck was modelled with an equivalent beam element in OpenSees, the stiffness of which was calibrated based on the results of a more precise beam-shell model constructed in CSI SAP2000. The variable stiffness of the deck due to changing thicknesses of the main girder flanges was considered by subdivision of the beam into several elements with varying properties. The pier and the two well foundations were also subdivided along their height into elements of length 0.1 m. Some elements were connected using rigid links due to the offset between their centroids, e.g. to support the deck at the location of the bearings and to connect the pier to the well foundations. The rigid elements were considered to be infinitely stiff and massless. The boundary conditions at the abutments were such to simulate the behaviour of the roller bearings, i.e. free translation in the longitudinal direction with rotations. Pairs of bearings at the pier were modelled as fixed against translation and were free to rotate.

3.2. Soil-structure interaction (SSI)

As mentioned previously, two different approaches were implemented with respect to modelling SSI (Fig. 4) as a result of the
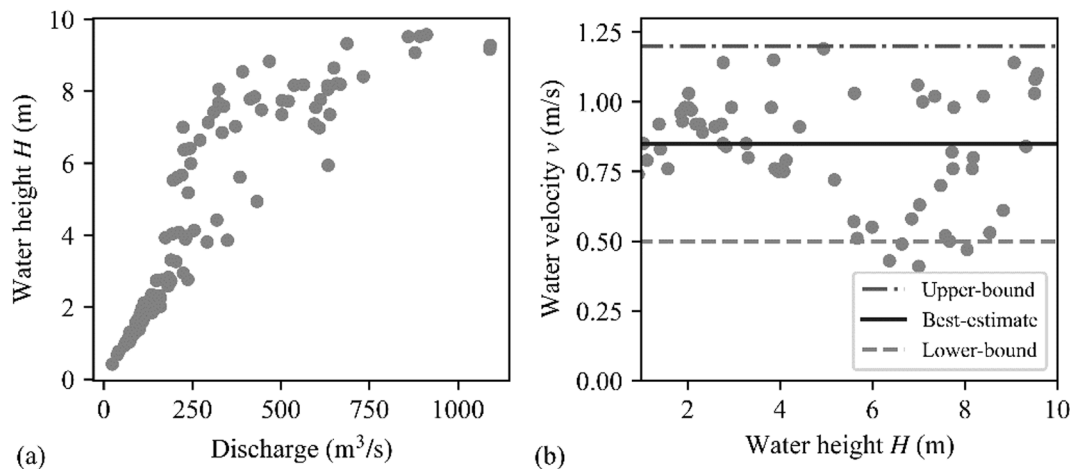

Fig. 3. Daily-max relations for numerical simulation of three flood events for years 2005, 2014 and 2015 – (a) Relationship between discharge and water height, (b) Relationship between water height and velocity, and three idealized scenarios.
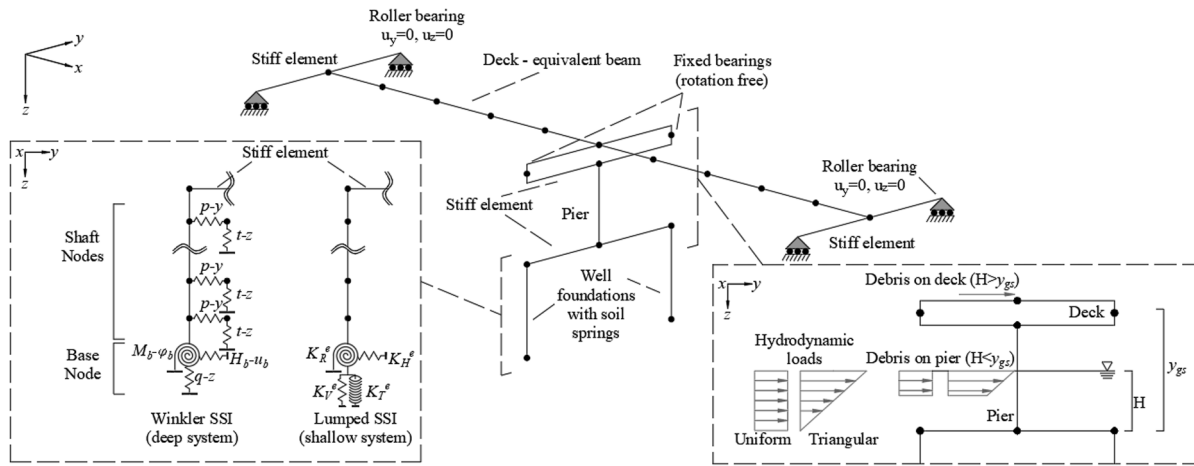
Fig. 4. Numerical model schematic of the modelled bridge.

uncertainty in foundation behaviour and the fact that the results of an operational modal analysis did not yield sufficient excitation in foundation modes to facilitate direct specification of SSI parameters. The first approach considers linear-elastic SSI with a set of lumped soil springs, termed herein as 'lumped-springs SSI model', while the second approach implements non-linear SSI with a set of distributed springs, termed 'Winkler-based SSI model'. Both approaches are described in the following sub-sections.

3.2.1. Lumped-springs SSI modelling (shallow system)

In the lumped-springs SSI modelling, it is assumed that the well foundation can be modelled as a shallow foundation. This assumption is justified by the small ratio between the foundation depth and its diameter ($\frac{L_f}{D_f} = \frac{5.8}{6.5} = 0.90$). In such cases, the SSI can be modelled using six mutually-independent springs located at the base of each foundation (Fig. 4). Several solutions exist for estimating the static stiffness of surface and embedded shallow foundations, see for example Refs. [51,52]. These solutions consider the soil as linear-elastic, the foundation as a rigid body, and the presence of a non-slip interface between the foundation and the soil. The influence of foundation embedment can be considered with modification factors that are applied to the solution obtained for surface foundations. In this paper, the equations for the static stiffness of embedded cylindrical foundations by Pais and Kausel [51] were used. The vertical (K_V), horizontal (K_H), rocking (K_R), and torsional (K_T), stiffness of the well foundation was computed as:

$$K_V^e = K_V^0 \left(1 + 0.54\, D_E/R_f\right) = \frac{4\,G\,R_f}{1-\nu}\left(1 + 0.54\, D_E/R_f\right) \tag{1}$$

$$K_H^e = K_H^0 \left(1 + D_E/R_f\right) = \frac{8GR_f}{2-\nu}\left(1 + D_E/R_f\right) \tag{2}$$

$$K_R^e = K_R^0\left(1 + D_E/R_f\right) = \frac{8GR_f^{\,3}}{3(1-\nu)}\left(1 + 2.3D_E/R_f + 0.58(D_E/R_f)^3\right) \tag{3}$$

$$K_T^e = K_T^0\left(1 + D_E/R_f\right) = \frac{16GR_f^{\,3}}{3}\left(1 + 2.67\, D_E/R_f\right) \tag{4}$$

where R_f and D_E are the radius and embedment depth of the foundation, while G and ν are the shear modulus and Poisson's ratio of the soil. The superscript e denotes the stiffness of the embedded foundation, whereas the stiffness of the equivalent surface foundation is denoted with superscript 0. It should be noted that the linear-elastic assumption adopted implies the model is only suited in the small to medium-strain range and is less accurate in large-strain fields, as experienced when the bridge is subjected to large loads. The spring stiffness should be reduced to incorporate non-linear behaviour at larger strains [53]. However, the

degree of the reduction is subject to some uncertainty [54]. For this reason, the model is applied in its unmodified form in this work.

3.2.2. Winkler-based SSI modelling (deep system)

In the second approach, the SSI is considered using distributed non-linear springs, which model lateral load–displacement (*p-y*), shear stress-vertical displacement (*t-z*), and base stress-vertical displacement (*q-z*) resistance mechanisms (see Fig. 4). As the well foundations have a small embedment ratio ($L_f/D_f = 0.90$), these traditional springs, originally developed for slender piles, were extended with the addition of a moment-rotation (M_b-φ_b), and a base shear-displacement spring (H_b-u_b), using the approach suggested by Van Impe and Wang [55]. A modification of the subgrade reaction of the *p-y* springs was necessary to account for the fact that the traditional approach does not consider the contribution of the shaft friction, which increases the stiffness, becoming important for rigid piles with low slenderness.

The load–displacement relationship of the *p-y*, *t-z* and *q-z* springs were modelled in OpenSees using *PySimple1* [56], *TzSimple1* [57] and *QzSimple1* [58] materials. The input parameters for definition of the materials are the ultimate forces (P_u, T_u, Q_u) and displacements at 50% of the ultimate force (y_{50}, z_{tz50}, z_{qz50}). The moment-rotation and load–displacement relationships of the M_b-φ_b and H_b-u_b springs were modelled using elastic-perfectly-plastic OpenSees material *ElasticPP* [59]. For the *p-y* springs, the backbone curve was derived according to API [60] recommendations, where the ultimate force (P_u) was computed according to Reese and Van Impe [61]:

$$P_u = \overline{A_s} p_u \, \Delta z \tag{5}$$

where $\overline{A_s}$ is the normalized resistance factor that depends on the ratio $\frac{z}{D_f}$, z is the depth of the spring, D_f is the foundation diameter, p_u is the ultimate soil resistance per unit length [61], and Δz is the vertical spacing of the springs. The displacement at 50% ultimate force was calculated based on the API [60] hyperbolic load–displacement curve:

$$y_{50} = \frac{\overline{A_s} p_u}{k\, z}\, \mathrm{atanh}(0.5) \tag{6}$$

where k is the coefficient of subgrade reaction, which depends on the soil density (and friction angle) and varies for saturated and unsaturated conditions. A preliminary study suggested that the stiffness obtained for the foundation was low compared to that derived using the lumped-spring SSI approach. Therefore, k was increased by a factor of 5 to match the modal characteristics of the lumped-spring SSI model. This is in line with recent findings from the PISA project, which suggests that non-slender foundations incur additional resistance mechanisms not accounted for by *p-y* springs alone [62], so adjusting the stiffness is a

crude way to account for some of this omitted resistance. It should be noted that this only affects the behaviour at very low strains, and the ultimate strength is unaffected by altering the initial stiffness.

The backbone curve for the t-z springs was defined according to Mosher [63], where the ultimate force of each spring was computed based on Mohr-Coulomb failure criteria:

$$T_u = K \sigma'_v \tan(\delta) \pi D_f \Delta z \tag{7}$$

where the coefficient of lateral pressure is taken as $K = 1.0$ (full displacement piles), σ'_v is the vertical effective stress, and δ is the friction angle of the soil-foundation interface, considered as $0.9\varphi'$. The displacement at 50% capacity (z_{tz50}) was assumed as 1.27 mm [64] for a bi-linear load–displacement relationship for sands.

The backbone curve of the q-z spring was defined according to the Vijayvergiya's [65] recommendations, where the ultimate bearing force at the tip of each well was computed according to Meyerhof [66] for shallow foundations ($D_E < D_f$):

$$Q_u = \left[c N_c d_c + \gamma D_E N_q d_q + 0.5 \gamma D_f N_\gamma d_\gamma \right] \pi \frac{D_f^2}{4} \tag{8}$$

where N_c, N_q, N_γ, and d_c, d_q, d_γ are the bearing and depth correction factors according to [66], respectively. The displacement (settlement) at 50% capacity was computed according to Burland and Burbidge's SPT method [67]:

$$z_{qz50} = q_{net,50} \frac{1.71}{\overline{N}_{60}^{1.4}} D_f^{0.7} \tag{9}$$

where $q_{net,50}$ is the net overburden pressure at 50% capacity (gravity loads are subtracted), and $\overline{N}_{60}$ is the average value of N_{60} blows in the influence zone of the foundation.

The initial rotational stiffness ($K_{\varphi b}$) of the M_b-φ_b spring at the base of the foundation was computed based on the solution for shallow foundations resting on elastic soil (e.g. [51]). The rotation at full mobilisation of the M_b-φ_b spring was computed as:

$$\theta_{pb} = \frac{M_{ub}}{K_{\varphi b}} = \frac{3 M_{ub}(1 - \nu)}{8(G R_f^3)} \tag{10}$$

where M_{ub} is the foundation ultimate moment capacity at the base, which was computed based on Meyerhof [66] using an iterative procedure whereby the applied moment was increased progressively until the soil reaction at the base could no longer support the applied load.

The initial stiffness of H_b-u_b spring (K_{hb}) at the base of the foundation was computed by dividing the ultimate sliding resistance (H_{ub}) by the displacement at full mobilisation of the resistance (u_{pb}). Considering the definition of H_{ub} [64], the initial stiffness K_{hb} is derived as:

$$K_{hb} = \frac{H_{ub}}{u_{pb}} = \frac{c' A_b + Q \tan \varphi'}{u_{pb}} \tag{11}$$

where c' and φ' are the effective cohesion and friction angle of the soil, A_b is the area of the foundation base, and Q is the applied vertical load on the foundation base. According to Van Impe and Wang [55], the sliding resistance can be considered to fully mobilise at a displacement (u_{pb}) of 5 mm.

3.3. Load modelling

The loads considered to act on the structure comprise gravity, hydrodynamic (drag force F_d and lift force F_l), buoyancy, and debris loads. The gravity load considers the self-weight of elements and permanent loads of finishes on the bridge deck. The hydrodynamic forces were computed according to Australian code AS5100.2–2004 [68]. The drag force in the direction of the flow (in kN) is defined as:

$$F_d = 0.5 C_d v^2 A_d \tag{12}$$

where C_d is the drag coefficient and A_d is projected wetted area in the direction of the flow. For piers with semi-circular shaped nose, C_d is 0.7. In the case of bridge decks, C_d is computed as a function of relative submergence of the deck (S_r) and proximity ratio (P_r), which are defined as:

$$S_r = \frac{d_{wgs}}{d_{sp}} \text{ and } P_r = \frac{y_{gs}}{d_{ss}} \tag{13}$$

where d_{wgs} is the distance from the deck soffit to flood water surface, d_{sp} is the wetted depth of deck (including any railing and parapets), y_{gs} is vertical average distance from the deck soffit to the riverbed, and d_{ss} is the wetted depth of the solid superstructure (excluding railing but including parapets).

The lift forces on the bridge pier and the deck (in kN) are computed as:

$$F_l = 0.5 C_l v^2 A_l \tag{14}$$

where C_l is the lift coefficient, and A_l is the projected wetted area in the direction perpendicular to the flow. In this study the lift force on the pier is neglected as the pier is oriented in the direction of the flow. The lift force on the submerged deck acts in the vertical direction. The coefficient C_l for bridge deck depends on the relative submergence of the deck (S_r). Two possible combinations of the lift force are prescribed: i) an upward lift force for the verification of overturning and calculation of tie-down forces, and ii) a downward force verification of the deck and foundations. For the purpose of this study, the lift forces on the deck were assumed to act in the upward direction and were combined with buoyancy.

Severe flooding can result in accumulation of debris on the bridge piers and superstructure. The debris forces were calculated according to Australian code AS5100.2–2004 [68], where the depth of the debris mat varies depending on factors such as catchment vegetation, available water flow depth, and superstructure span. The standard AS5100.2–2004 specifies the depth of the debris mat to be between 1.2 m and 3 m. In this study rectangular debris with an average depth of 2.1 m was assumed.

In the case of bridge piers, the length of the debris mat is assumed to be equal to one half of the sum of the adjacent spans or 20 m, whichever is smaller. The top of the debris mat is assumed to be located at the top of the flood level. In case of the bridge deck, the projected length of the debris mat is equal to the projected length of deck. The loads are applied at the mid-height of the deck, including any railing or parapets. The debris forces are calculated with Equation (12) considering separate drag coefficients (C_d) for bridge piers and decks. Both factors depend on H and v. The factor C_d for debris on the deck depends additionally on the proximity ratio (P_r).

The loads are combined to produce the maximum possible overturning action on the bridge, which is considered to occur when horizontal hydrodynamic and debris loads are combined with an uplift action on the deck. Traffic loads were omitted from the analysis as it is assumed that the bridge under this combination of loads would be closed to traffic [39]. Hydrodynamic loads were only applied to the areas of the bridge not affected by debris (i.e., no concurrent action with the debris is expected). The reason for this is that in the Australian code [68], loads caused by debris include the contribution from the hydrodynamic loads, so these are omitted in the presence of debris to avoid duplication. The loads were calculated per unit length of individual components and were applied in the model as uniformly distributed loads.

3.4. Scour modelling

For each flood scenario, the depth of local pier scour was computed

according to the HEC-18 [69]:

$$y_s = \left[2.0\,K_1\,K_2\,K_3 \left(\frac{H}{a}\right)^{0.35} Fr^{0.43} \right] a \qquad (15)$$

where K_1, K_2, K_3 are correction factors for pier nose shape, angle of attack of flow (θ), and riverbed conditions, respectively, and a is the pier width. F_r is the Froude number defined as:

$$F_r = \frac{v}{(g\,H)^{1/2}} \qquad (16)$$

where g is the acceleration of gravity. For round-nose piers and angle of attack of flow $\theta = 0$, the coefficients K_1 and K_2 amount to 1.0. For clear-water scour, K_3 is 1.1.

In the case of the Winkler SSI approach, the effect of local pier scour was modelled by not assigning SSI springs, defined in Section 3.2.2, to the part of the foundation exposed by scour [13,15,31]. This results in a decrease in the horizontal stiffness and increase of vertical settlement of the bridge due to a smaller embedded length of the foundation. A slightly different approach was used in the case of the lumped-spring SSI approach, described in Section 3.2.1, where the effect of scour was considered to affect the embedment depth of the foundation and this resulted in a change of the static foundation stiffness. Some issues related to these modelling assumptions are that it is very difficult to account for the shape of local scour holes using this approach, or even to differentiate between local and global scour, as changes in embedment and not assigning stiffness to surface springs amount to the removal of a uniform soil layer. This leads to uncertainty in how scour hole shape affects the bridge [70]. Previous research [71–74] has shown that the shape of the local scour holes exhibit some influence on the foundation response due to the presence of overburden near the scoured foundation. The presence of this overburden is crudely accounted for by not altering the ultimate bearing resistance of the base springs (Equation (8)) to account for some of the locked-in stresses in the Winkler-based SSI model. It should be noted that this simplification is a result of how scour is modelled using spring-beam models, and there is limited research on quantifying the overburden that remains for various local scour hole shapes.

In addition to the effect on the stiffness of the foundation, local pier scour can lead to exposure of the foundation to additional hydrodynamic flow loads, as the foundation is no longer shielded by soil. This effect was considered by assigning additional drag forces on the scoured part of the foundation. Furthermore, debris accumulation against the pier can result in an increase in scour depth due to constriction and redirection of the water flow. The effect of debris on the local scour of the pier was considered according to the recommended approach proposed by Lagasse et al. [19], which relies on the quantification of the equivalent pier width (a_d^*) that is subsequently used in Equation (15) for quantification of the scour depth with consideration of debris. The equivalent pier width is defined as:

$$a_d^* = \frac{K_{d1}(T_d W_d)(L_d/H)^{K_{d2}} + (H - K_{d1}\,T_d)a}{H} \text{ for } L_d/H > 1.0$$

$$a_d^* = \frac{K_{d1}(T_d\,W_d) + (H - K_{d1}\,T_d)\,a}{H} \text{ for } L_d/H \le 1.0 \qquad (17)$$

where K_{d1} and K_{d2} are experimentally obtained factors, which depend on the shape of the debris raft ($K_{d1} = 0.79$ and $K_{d2} = -0.79$ for rectangular debris raft), W_d is the width of the debris raft normal to the flow, T_d is the thickness of debris raft, and L_d is the length of the debris upstream from the pier face. In the study, the length of the debris was assumed to be equal to the water height ($L_d/H = 1.0$), which produces the largest amplification of scour for a given water height.

4. Analysis and results

This section contains a critical analysis of the influence of various load effects on the response of the modelled bridge.

4.1. Model verification

Outputs from the developed numerical models with both SSI configurations were compared to measured periods obtained from the ambient modal survey of the bridge in order to identify deviations in modelled behaviour. It should be noted that a direct validation of the SSI modelling was not possible due to the inability to measure the bridge's translational modes, so the modal periods for the translational modes of the SSI models could not be validated, and only the modal periods of the bridge deck are validated against the measured values from Section 2.4. The comparison of the first 7 calculated modal periods from both models with the available measured data is presented in Table 3. The modal periods from a Fixed-base model, with no SSI, is also shown for comparison.

The results of Table 3 exhibit excellent agreement between the calculated and measured modal periods of the bridge deck. The modelling of SSI is found to have small influence of the vibration modes of the bridge deck, as all modelling approaches resulted in a similar modal behaviour of the bridge with a good match of the modal periods. This is however not the case for global translational modes, for which the modelling of SSI resulted in more flexible behaviour (larger modal periods) compared to the Fixed-base model. A slight difference was also obtained for the modal period of the vertical mode, for which the Winkler SSI resulted in a somewhat larger modal period compared to the Lumped SSI model, indicating that the employed Winkler SSI modelling facilitates slightly more flexible behaviour in the vertical direction.

4.2. Flood analysis

The results of the flooding analysis for different modelled scenarios are presented herein, which comprise: (i) analysis of the total horizontal loads and internal forces of individual bridge members, (ii) analysis of the effect of scour on modal periods, (iii) the assessment of utilization ratios of bridge members, and (iv) analysis of the required conditions to result in bridge failure for different flooding scenarios. The effect of debris-induced amplification of scour on the bridge response is also

Table 3

Comparison of the Fixed-base, Lumped SSI and Winkler SSI model with measured modal periods.

No.	Description	Period (s) – Fixed-base model	Period (s) - Lumped SSI model	Period (s) - Winkler SSI model	Period (s) - Measured
1	1st vertical mode of the deck	0.66	0.67	0.67	0.68
2	Global longitudinal mode	0.23	0.58	0.60	ND
3	2nd vertical mode of the deck	0.40	0.41	0.42	0.43
4	Global transverse mode	0.20	0.36	0.36	ND
5	Global vertical mode	*	0.21	0.24	ND
6	1st transverse mode of the deck	0.21	0.21	0.21	0.21
7	3rd vertical mode of the deck	0.18	0.18	0.18	0.19

ND – not detected based on ambient vibration measurements.

* this mode shape is already identified within the 2nd vertical mode of the deck.

analysed by means of a subsequent sensitivity analysis.

4.2.1. Total horizontal loads for different flooding scenarios and flow distributions

Table 4 presents the horizontal forces experienced by the bridge for two different distributions of flow forces, i.e. rectangular and triangular. The purpose of this was to examine the difference between the rectangular distribution specified in the Australian code [68] and the triangular distribution used in similar flood analyses [75–77]. For each distribution of forces, four different load conditions are considered, with and without scour, as well as with and without debris (interaction of debris and scour is considered in a subsequent sensitivity analysis). Forces increase with water height and velocity. The largest increase occurs when water reaches the deck ($H = 10$ m, elevation of deck is 8.15 m), and is greatest for the case where the flow velocity is 1.2 m/s. The results for this flow velocity are presented in Fig. 5.

Debris significantly increases the loading on the bridge whereby the relative contribution is largest for the lower water heights (4 m and 8 m). This is a result of debris 'blocking' a relatively larger portion of the river flow at lower heights. For the case when water reaches the deck, the increase resulting from debris is smaller but still amounts to about 80% relative to the case without debris, regardless of whether scour is considered or not. Scour increases the loading as a result of exposing the foundations, the relative contribution of this is largest for lower water heights. When combined with debris, the relative increase of the total flood load is somewhat lower.

The triangular distribution of flow velocity results in the same or increased loading in general (relative to the rectangular distribution), except for the case where there is no debris with scour below $H = 10$ m. A significant relative increase occurs when water reaches the deck ($H = 10$ m) and when debris is considered. This is likely a result that the triangular distribution has a relatively larger velocity at the water surface compared to the rectangular distribution, which subsequently has a larger influence when it meets the deck.

4.2.2. Effect of local scour on modal periods of the bridge

The effect of local scour at the pier on the lateral modal periods of the bridge is examined herein, whereby several flooding scenarios are considered by varying water height and velocity. The obtained scour depth calculated according to Equation (15) are presented in Fig. 6. The two SSI modelling approaches are compared in Fig. 7, which shows how scour depth at different water heights affects the first modal periods of the bridge in the x- (traffic) and y- (flow) directions. Scour leads to an

increase in both horizontal vibration periods ($T_{1,x}$ and $T_{1,y}$). The effect is larger in the x-direction because the foundation and pier act like a cantilever as a result of the roller bearing connections at both ends of the deck. In the transverse direction, the effect is smaller because most of the foundation stiffness comes from the coupling effect of the two well foundations.

In the x-direction, the Winker model results in slightly larger modal periods for a given water height as compared to the Lumped SSI model. In the y-direction, however, the opposite is observed. This is likely a result of the fact that in the lumped SSI model, the change of embedment depth has a larger impact on both vertical and rotational stiffness, whereas in the Winkler model, the removal of the p-y and t-z springs has a negligible effect on the vertical stiffness of the well, as most of the load is transferred by the tip. In the y-direction, due to the governing nature of the pile coupling effect, the impact is lower.

The results presented in this section are broadly in line with many previous studies who have reported similar findings, namely that scour increases modal periods (or decreases natural frequencies), e.g. [13,20,22,33,78]. It should be noted that the lumped-spring SSI model is only valid in the small to medium strain range so larger scour effects are likely under-predicted using this model.

4.2.3. Internal forces of bridge members under different scenarios

The internal forces within bridge members are analysed for the case where the flow velocity is 1.2 m/s, as this was the most critical scenario in Section 4.2.1. Such scenario is expected to produce the largest internal forces and utilization ratios of the bridge members. Fig. 8 and Fig. 9 present the results for the bending moments and shear forces experienced at the base of the bridge pier, for both flow force profiles (rectangular and triangular), and both foundation modelling approaches. For ease of visualisation, the internal forces are shown as resulting from flood loads only (gravity loads are omitted).

Fig. 8(a) shows the bending moment at the base of the pier as a function of water height under a rectangular force distribution for four cases, with and without scour, and in the presence and absence of debris, for the model with lumped SSI properties. Fig. 8(b) shows the same information but for a triangular force distribution. Fig. 8(c) and (d) show the same data but for a Winkler SSI scheme.

In Fig. 8, it can be seen that the pier bending moment increases significantly when the water height reaches the bridge deck ($H > 8.15$ m). In the absence of debris, the bending moment is almost negligible when the water is below the deck for all cases, whereas the presence of debris increases the bending moment significantly. The first increase (change in slope) occurs when the water height exceeds the assumed depth of the debris mat (below this depth, debris is not considered present). A second increase occurs when the water height meets the deck. For the triangular distribution in Fig. 8(b) and (d), the bending moments reduce once the water height exceeds 10 m as a result of over-topping of the deck. When the water height reaches 12 m, the results are the same as the case where there is no debris.

The difference between the scour and no scour conditions is minimal as compared to the differences caused by debris presence, suggesting the internal forces in the bridge as a result of local scour are not severe. When water is below the deck, the presence of scour leads to an increase in the bending moment in the pier. The opposite is true when the deck is submerged, as scour appears to slightly decrease the demand on the pier. In the former case, the increase in the demand on the pier is a result of additional hydrodynamic loads being applied to the pier due to the foundation being exposed by scour. However, scour also reduces the stiffness of the pier, which causes more loading to be redistributed to the bridge deck once the deck is fully submerged, which results in a later reduction of the demand in the pier. This explains why the 'no scour' condition is actually more severe in terms of bending in the bridge pier than the scoured condition [18]. The model does not take into account accumulated displacements or rotations caused by the lowering stiffness.
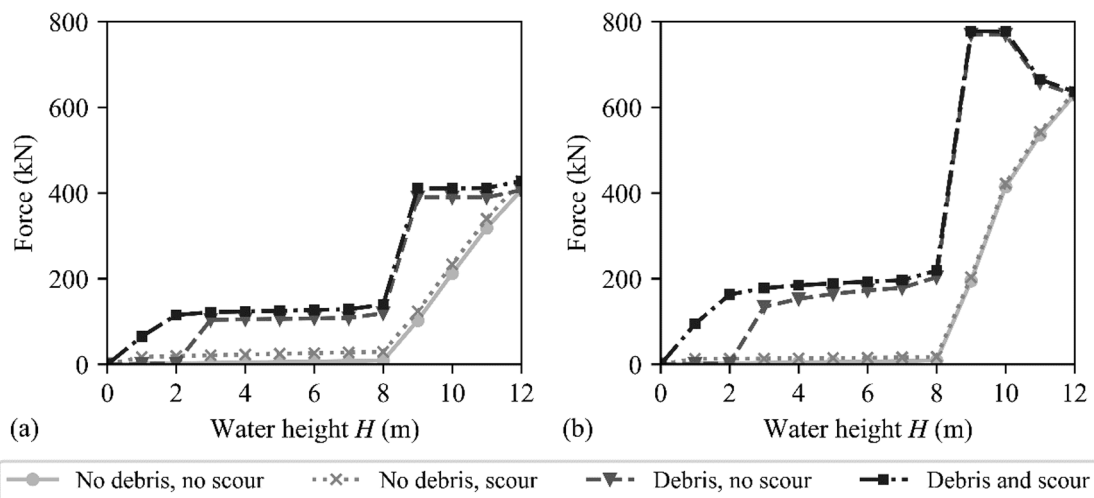
Table 4

Total horizontal loads (kN) for different flooding scenarios.

Uniform distribution of flow forces					
H (m)	v (m/s)	No debris, no scour	No debris, scour	Debris, no scour	Debris and scour
4	0.5	1	3	18	20
	0.85	2	10	53	61
	1.2	4	23	105	123
8	0.5	2	4	21	23
	0.85	4	13	60	69
	1.2	9	29	119	139
10	0.5	37	39	68	70
	0.85	106	116	195	205
	1.2	212	233	390	411
Triangular distribution of flow forces					
4	0.5	1	2	26	30
	0.85	2	6	77	91
	1.2	4	14	153	184
8	0.5	2	2	35	37
	0.85	4	8	102	108
	1.2	9	17	203	219
10	0.5	72	73	134	134
	0.85	208	211	386	389
	1.2	414	422	769	777

Fig. 5. Total horizontal loads for different flooding scenarios at flow velocity of 1.2 m/s considering (a) rectangular and (b) triangular distribution of flood forces.
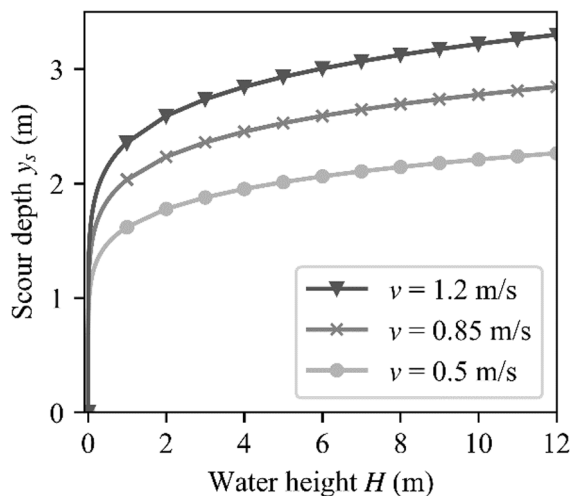

Fig. 6. Calculated scour depths y_s for different flooding scenarios defined by water height and flow velocity.

In general, the triangular distribution leads to a higher demand on the pier than the rectangular distribution as a result of the less favour-able distribution having more loading applied nearer the top. The results obtained with both SSI modelling approaches are similar, although the Winker SSI model produced slightly larger demand on the pier.

Fig. 9 shows the same data as Fig. 8, but this time for the shear force generated at the base of the pier. The trend in the results is similar to that of the bending moment in Fig. 8, in that the shear forces increase with increasing water height. The presence of debris induces more severe shear forces than in the absence of debris in all cases. When the water height is lower than the bridge deck, scour results in higher shear forces due to the increased forces applied as a result of the removed material due to the scour hole. However, similar to the case of bending, scour increases the pier flexibility causing more forces to be distributed to the deck when the water height reaches this level, meaning that the shear forces at the base of the pier are lower for the case where water height exceeds the deck height in the presence of scour relative to no scour. This is a somewhat counterintuitive finding, but implies that scour may have some unintended beneficial effects of reducing internal stresses in elements due to increased flexibility. As above, however, accumulated displacements and rotations are not considered in this model, which may counteract any benefit.

Fig. 10 shows the transverse bending moment in the centre of the

first span of the deck for both foundation models and flow distributions, under increasing water heights in the presence and absence of debris and scour. Results show that the greatest change in bending moment occurs when the water height reaches the deck level as is expected. In the absence of debris, the bending moment increases slowly until the water reaches the deck, where it rises sharply. This is true for both foundation models and flow distributions. Similar to previous results, the effect of scour is different for water below deck level and exceeding deck level, due to the change in the flexibility of the system resulting from scour. However, the opposite trend is observed in this case relative to the pier – for water height below the deck, scour results in a lower moment, whereas when water height exceeds the deck, the scoured moment is higher. This is a result of scour reducing the pier stiffness meaning more load is distributed to the deck.

The results of the shear forces in the pier and abutment bearings, foundation tip axial forces, and foundation tip moments are shown as supplementary information in Appendix A.

4.2.4. Utilization ratios of bridge members for different flood scenarios

This section presents an analysis of the utilization ratios of the bridge members for different flooding scenarios, which are defined as the ratio between the demand for combined gravity and flooding loads, and the unfactored capacity. As unfactored capacity is used, it should be noted that the results in this section would be more critical if factors were considered. Failure of the bridge is assumed to occur when the utilization ratio of a component exceeds a value of 1.0. The analyses of the utilization ratios was performed for the most critical flooding scenario, which according to the results of previous sections is obtained for the flow velocity of 1.2 m/s and the triangular force distribution. Such a scenario is expected to produce the largest internal forces and, ergo, utilization ratios of the bridge members.

A preliminary study indicated that the utilization ratios for the bridge deck and the foundation are very low, suggesting the capacity far exceeds the demand. As a result, these analyses are omitted from the paper for brevity. In addition, both foundation models exhibited similar behaviour so only the results from the Winkler SSI model are presented. The pier bending capacity was conservatively defined based on the section modulus and mean tensile strength of concrete C25/30 according to EN- 1992–1-1 [41]. The effect of reinforcement was not considered, because it was assumed that the amount of reinforcement is below minimum code requirements [41]. The shear strength of the pier was calculated according to Equation (6.2.a) from EN- 1992–1-1 [41], which is applicable for members without shear reinforcement. Shear capacities of the shear pin at the middle bearing and the shear keys at the abutment bearing were computed considering the elastic shear resistance
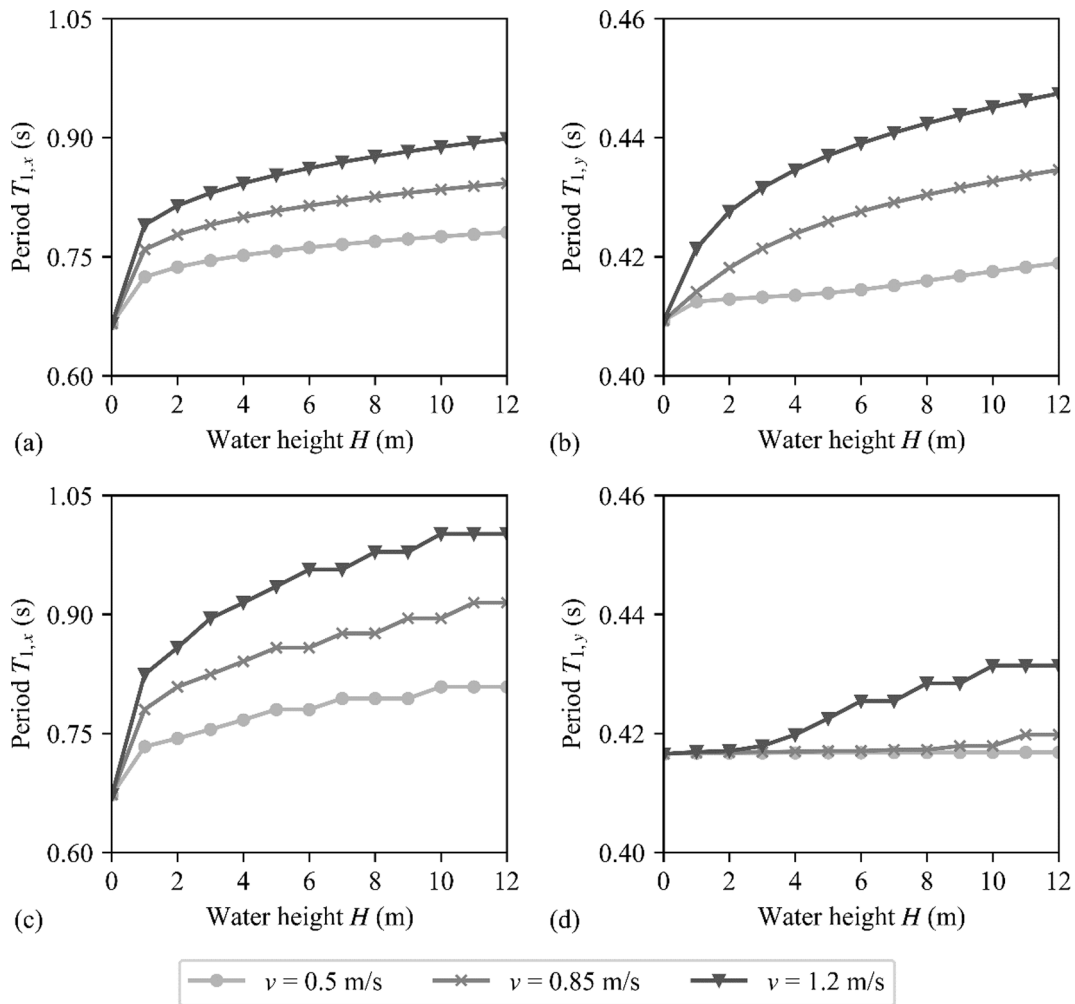
Fig. 7. Effect of local scour (at different water heights) on first modal periods in x and y direction of the bridge for different flooding scenarios and two SSI modelling approaches: (a,b) Lumped SSI modelling and (c,d) Winkler SSI modelling.

according to EN-1993–1-1 [40], assuming a yield strength of steel of 235 MPa.

Table 5 presents the utilization ratios of different bridge elements for different flood scenarios. The largest utilization ratios were obtained for the bearing above the pier (data in Appendix A). However, none of the utilization ratios exceeded 1.0 so failure of the bridge was not attained. The utilization ratios of the bearing above the pier increase significantly when water reaches the deck. For water height below the deck level and in presence of debris, the largest utilization ratios were obtained for the pier in shear (though these are low relatively). The presence of debris on the bridge increases the utilization ratios of the pier bearing by almost 75%. The presence of scour slightly increases the utilization ratios of the pier bearing for water height below the deck level ($H = 4$ m, 8 m). On the contrary, scour is observed to slightly decrease the utilization ratios for pier bearings in the case where the water height reaches the deck (0.73 vs 0.77 in presence of debris and 0.42 vs 0.44 without debris). This result is a consequence of scour increasing the system flexibility. Consequently, less load is carried by the bearing above the pier.

4.2.5. Analysis of bridge failure for different flood scenarios

The analyses in the previous section showed that bridge failure does not occur under the considered scenarios. An additional study is performed herein to estimate the flow velocities that would be required to reach failure under given scenarios. The goal of the study is also to identify the critical elements leading to failure of the bridge with respect to different flooding scenarios. For each of the examined situations, the

flow velocity was increased iteratively until the first element fails, or scour depth exceeds the foundation depth, whichever occurs first. The resulting flow velocities at failure are presented in Table 6. It should be noted that in many cases the attained flow velocity is entirely unrealistic, which implies failure is highly unlikely, so the results should be considered in this respect.

Table 6 shows that failure of the bridge due to flood loads only (with no debris and no scour) is highly unlikely for water levels below the deck ($H = 4$ or 8 m), i.e. very high flows are required to induce failure. Once the deck is submerged ($H > 8.15$ m), the required flow velocity to cause failure drops significantly to values between 1.4 m/s and 3.2 m/s, which are not expected based on the considered hydrological data, but are not unrealistic values that could occur. The most critical scenarios were obtained for the presence of debris and/or local pier scour, which reduce the required flow velocity to reach failure. In flood scenarios with water below the level of the deck, the presence of scour was found to significantly reduce the required velocity to reach failure, which was especially evident for the analyses performed without debris (80% reduction). In the analyses with debris, the reduction was in the order of 40%. This is indicative of how damaging scour can be in terms of reducing the reliability of the bridge.

In the majority of the scenarios, the 'failure' of the bridge resulted from failure of the bearing above the pier, which in real terms can result in deck unseating. In some cases, failure of the bridge was related to scour exceeding the depth of the foundation, which was conservatively considered as failure and was not possible to model within the numerical
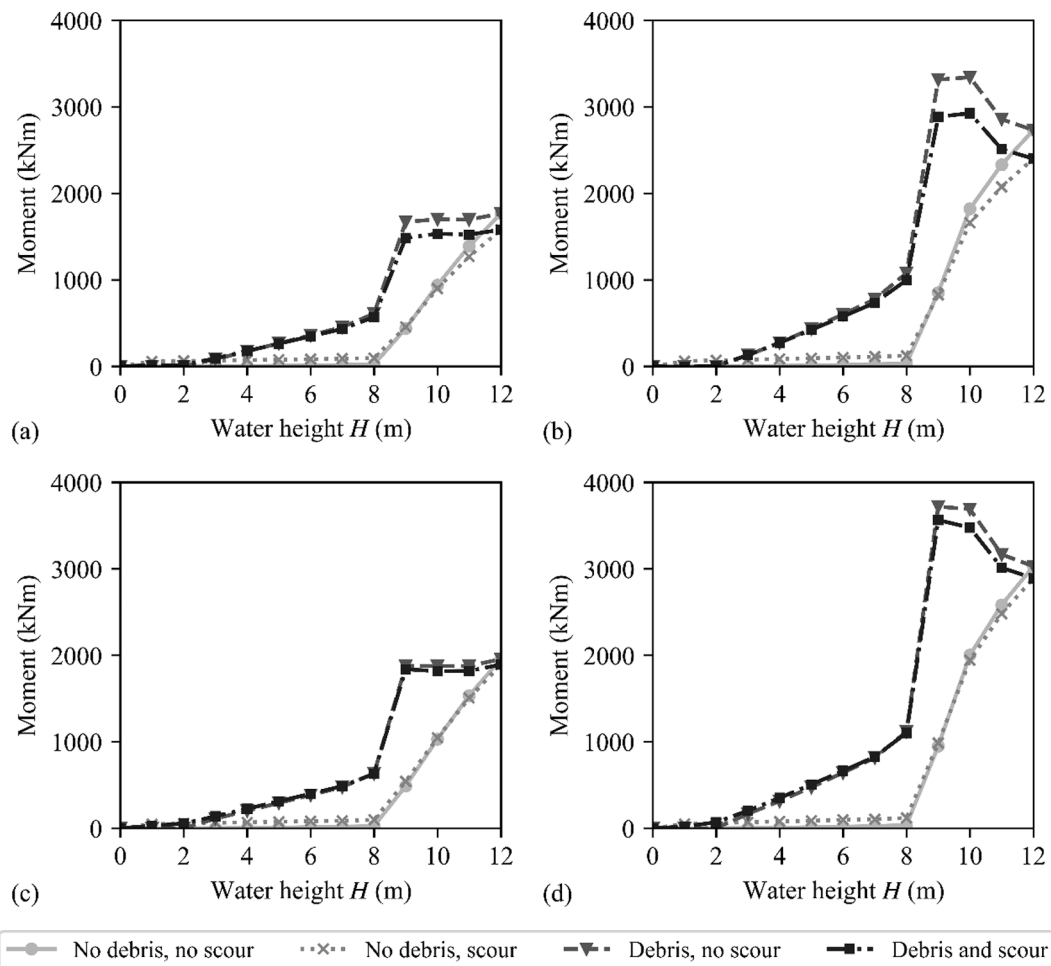
Fig. 8. Pier bending moment due to flood load with consideration of rectangular and triangular distribution of flow forces for (a,b) the Lumped-spring SSI model and (c,d) the Winkler-spring SSI model with consideration of different flooding scenarios ($v = 1.2$ m/s).

scheme due to the loss of boundary support. The cases where scour led to failure when water height is below the deck level occur with water velocities of about 5 to 6 m/s. Such scenarios could feasibly occur if large debris accumulation obstructs the flow of the water, leading to a local increase of the flow velocity near the pier. Such scenarios were taken into consideration within an additional sensitivity analysis, which explicitly considered the amplification of scour due to the effect of debris. Additional details are provided in section 4.2.6.

4.2.6. Failure of the bridge due to debris-induced amplification of scour

In this section, failure of the bridge due to debris-induced amplification of scour is examined. In Fig. 11, the scour depth computed with consideration of debris in accordance with Section 3.4 is compared to the total depth of the foundation (5.8 m), which is marked with a dark grey dashed line. Several flooding scenarios with respect to flood height and velocity are considered. For demonstration purposes, a simplified bridge failure is assumed to occur when the scour depth reaches the base of the foundation, although it is acknowledged that the foundation would at this point still be able to provide additional support to the bridge. The purpose of this study is to highlight the most critical scenarios with respect to scour and related interaction with consideration of debris presence.

Fig. 11(a) shows the scour depth as a function of water height and velocity, derived using Equation (15). Fig. 11(b) shows the scour depth derived in the presence of debris. As can be seen from Fig. 11, debris can result in significant amplification of the scour depth for a given velocity and water height. It is noteworthy that the greatest amplification does

not occur for the largest water height; rather for larger water heights, scour actually decreases. This is a function of the relative blockage to the flow, which is more pronounced at lower water height, resulting in larger amplification of flow velocity. The largest scour depth is obtained for a flood height of 3 m. In this scenario, failure of the pier is expected to occur at a lower flow velocity of 0.5 m/s, whereby the scour depth exceeds the foundation depth. It can be concluded that debris accumulation can significantly increase the likelihood of scour-related failure of bridges, as the critical situation could be achieved at more commonly experienced water heights.

5. Conclusions

In this paper, an analysis of the responses of various components of a roadway bridge under scour and debris-loading is undertaken. A numerical model of the bridge is developed in OpenSees, and two modelling approaches are used for the SSI; a lumped-springs SSI model, and a Winkler-based SSI model. The model is exposed to gravity, hydrodynamic, buoyancy, and debris loads. Scour hole depth is computed based on hydraulic flow data using equations from the literature. The results of a modal survey on an actual bridge are used to validate the numerical model performance prior to conducting the analyses.

A flood-analysis is conducted whereby the response of the bridge is assessed in terms of total horizontal and internal forces, utilization ratios (capacity vs demand), modal periods, and failure loads under various scour conditions and presence of debris. In terms of applied horizontal forces on the bridge, two different flow force distributions were
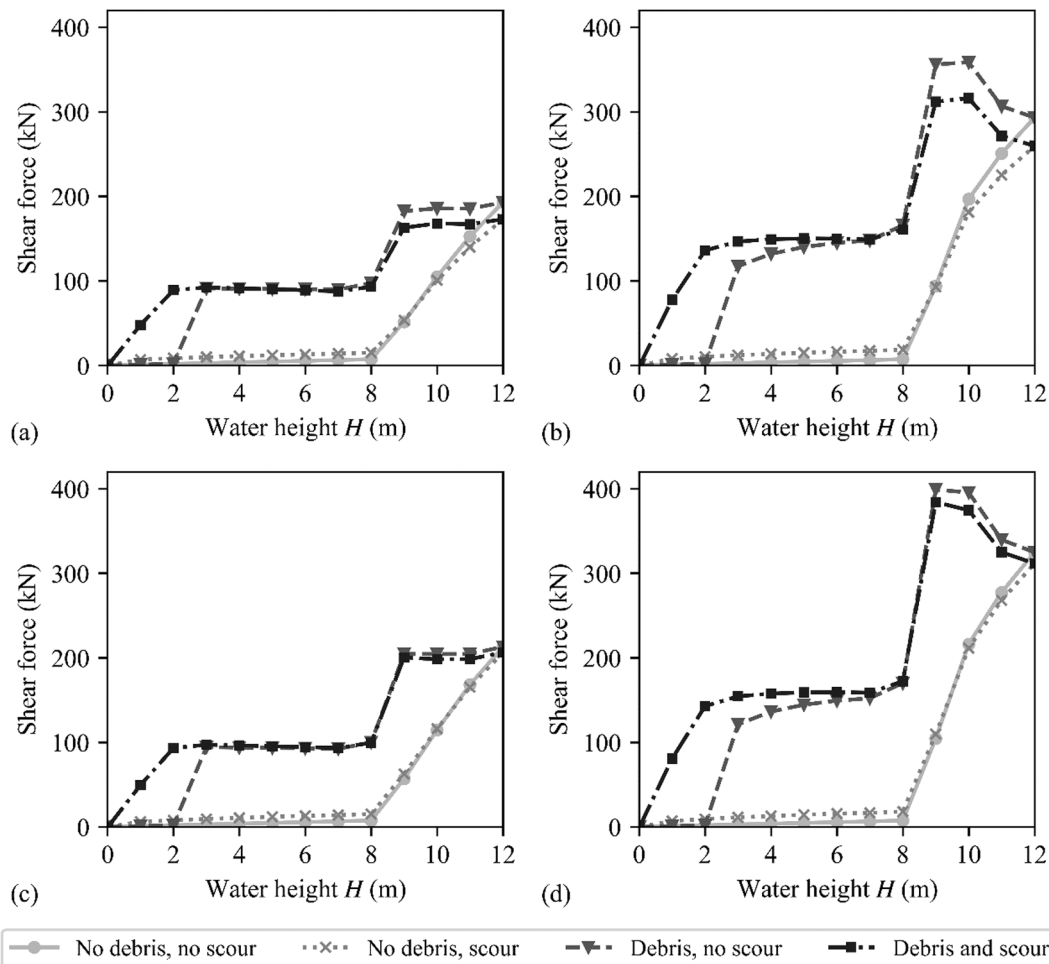
Fig. 9. Pier shear force due to flood loads for uniform and triangular distribution of flow forces for (a,b) the Lumped-spring SSI model and (c,d) the Winkler-spring SSI model with consideration of different flooding scenarios (*v* = 1.2 m/s).

considered, rectangular and triangular. Forces increase with water height and velocity as expected, with the largest increase occurring when the water reaches the height of the deck. Debris increases loads on the bridge, especially for lower water heights (due to the effect of blocking the flow path). Scour increases loading by exposing the foundations. The triangular distribution generally has higher loading effect on the bridge due to more load concentrated near the surface. Scour increases the modal periods (reduces frequency) in both horizontal directions, with a larger effect in the traffic direction than the flow direction due to the presence of roller bearings each end of the deck.

In terms of internal forces due to flood-loads, the bending moment at the base of the pier increases when the water height reaches the deck. For water heights below deck level, in the absence of debris the bending moments are negligible, becoming more significant in the presence of debris. Bending moments reduce for the triangular force distribution when water height overtops the deck. For water heights below deck level, scour increases the pier bending moment due to the additional hydrodynamic loads applied on the exposed foundation. When water height overtops the deck, scour presence reduces the demand on the pier through a redistribution of load from the pier to the deck as a result of the reduced pier stiffness from the scour hole. This finding counterintuitively suggests that scour may have some unintended benefits for certain bridge elements under severe hydraulic loading. However, this benefit is likely to be significantly outweighed by the development of accumulated permanent settlement and rotation of the structure, which could not be modelled using the SSI framework in this work. The shear force at the base of the pier exhibits a similar trend to the bending

moment. Debris presence leads to larger shear forces. Scour has the same effect on shear as it does on bending moment, in that it leads to a reduction in shear force when water exceeds the deck height compared to the case where there is no scour. In terms of deck bending moments, these are mostly influenced by whether water is below or at deck level. Scour presence has the opposite effect on the deck than on the pier due to how loads are redistributed from the pier to the deck due to the reduced pier stiffness.

An analysis of utilization ratios suggests that the bridge will not fail under scour from the applied hydraulic loads considered. The bridge deck and foundation exhibit very low utilization ratios. The bridge bearings exhibit the highest ratios, but do not exceed 1.0 and hence are not expected to fail. Debris can increase the utilization ratio significantly. The presence of debris can also magnify the expected scour depth substantially, and is actually more severe for lower water heights due to blocking of the flow exacerbating flow velocity. This implies that debris presence is likely to result in significantly more damage to a bridge under scour than in the absence of debris, and failure can occur at even low flow velocities.

The foundation models adopted in the paper could not be directly validated as it did not prove possible to obtain the appropriate modal data in a conducted survey. As a result, two different foundation models were implemented, and it should be acknowledged that these have inherent limitations, particularly the lumped-spring SSI model, which is only valid at small to medium strains. The results of the analyses at larger strains likely over-predict the strength and under-predict the increase in modal periods, as the strain-dependence in stiffness is not
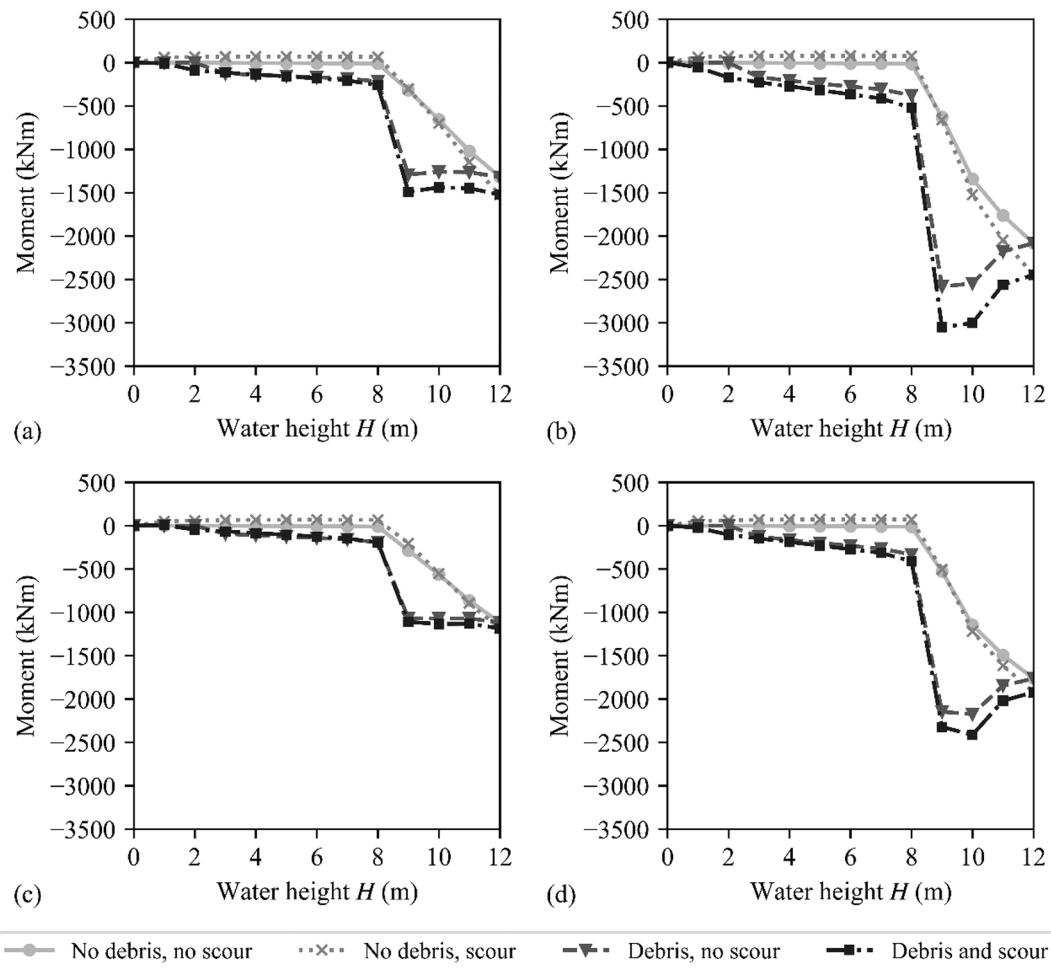
Fig. 10. Transverse bending moment due to flood loads of the deck for uniform and triangular distribution of flow velocity for (a,b) the Lumped-spring SSI model and (c,d) the Winkler-spring SSI model with consideration of different flooding scenarios ($v = 1.2$ m/s).

Table 5
Utilization ratios of bridge members for different flood scenarios ($v = 1.2$ m/s) obtained with the Winkler SSI model.

No debris, no scour				
H (m)	Pier in bending	Pier in shear	Pier bearings in shear	Abutment bearings in shear
4	0.02	0.00	0.04	0.01
8	0.02	0.00	0.04	0.01
10	0.01	0.04	0.44	0.09
No debris, scour *				
H (m)	Pier in bending	Pier in shear	Pier bearings in shear	Abutment bearings in shear
4	0.02	0.01	0.06	0.02
8	0.02	0.01	0.06	0.02
10	0.01	0.04	0.42	0.09
Debris, no scour				
H (m)	Pier in bending	Pier in shear	Pier bearings in shear	Abutment bearings in shear
4	0.02	0.03	0.01	0.00
8	0.01	0.03	0.03	0.00
10	0.01	0.07	0.77	0.18
Debris and scour *				
H (m)	Pier in bending	Pier in shear	Pier bearings in shear	Abutment bearings in shear
4	0.02	0.03	0.01	0.00
8	0.01	0.03	0.04	0.01
10	0.01	0.06	0.73	0.19

* $y_s(H = 4m) = 2.84m, y_s(H = 8m) = 3.12m, y_s(H = 10m) = 3.22m$

incorporated. The results should be understood qualitatively for larger-strain analyses, and future work will undertake a more comprehensive large-strain analysis with more appropriate stiffness modification.

The work in this paper should be of interest to bridge asset managers tasked with decision-making around remediation and resilience assessment of bridges on transport networks. Additional future work will focus

Table 6

Flood velocities resulting in failure of the bridge (in m/s) for different flood scenarios and two distributions of flow forces (Winkler SSI model).

Uniform flow distribution				
H (m)	No debris, no scour (m/s)	No debris, scour (m/s)	Debris, no scour (m/s)	Debris and scour (m/s)
4	44.5	6.4*	12.9	6.2*
8	26.4	5.1*	9.2	5.1*
10	2.7	3.2	2.0	2.2
Triangular flow distribution				
H (m)	No debris, no scour (m/s)	No debris, scour (m/s)	Debris, no scour (m/s)	Debris and scour (m/s)
4	42.5	6.4*	10.7	6.1
8	23.9	5.1*	7.0	4.8
10	1.9	2.1	1.4	1.5

* Failure related to scour exceeding foundation depth.
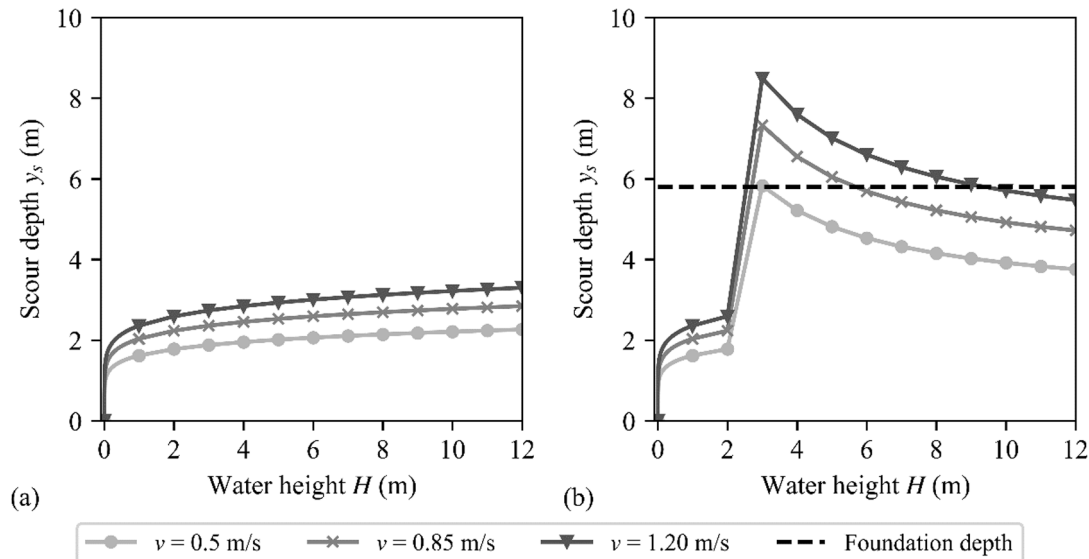
Fig. 11. Comparison of scour depths for different flood scenarios obtained (a) without and (b) with consideration of the amplification due to effect of debris.

on expanding the modelling approach to investigate combined hazards of earthquakes and scour occurrence.

CRediT authorship contribution statement

M. Kosič: Conceptualization, Methodology, Visualization, Software, Formal analysis, Writing – original draft. **L.J. Prendergast:** Conceptualization, Methodology, Visualization, Writing – review & editing. **A. Anžlin:** Conceptualization, Methodology, Writing – review & editing, Funding acquisition.

Declaration of Competing Interest

The authors declare that they have no known competing financial interests or personal relationships that could have appeared to influence the work reported in this paper.

Data availability

Data will be made available on request.

Appendix A. Supplementary material

Supplementary data to this article can be found online at https://doi.org/10.1016/j.engstruct.2023.115607.

References

[1] Pachauri RK, Allen MR, Barros VR, Broome J, Cramer W, Christ R, et al. Climate change 2014: synthesis report. Contribution of Working Groups I, II and III to the fifth assessment report of the Intergovernmental Panel on Climate Change. Ipcc; 2014.

[2] United Nations. COP 26. UN Clim Chang Conf; 2021.

[3] Matos JC, Casas JR, Fernandes S. COST Action TU 1406 quality specifications for roadway bridges (BridgeSpec) 2016.

[4] Hamill L. Bridge Hydraulics. London: E. & F.N. Spon; 1999.

[5] Maddison B. Scour failure of bridges. Proc ICE - Forensic Eng 2012;165:39–52.

[6] Melville BW, Coleman SE. Bridge scour. Highlands Ranch, CO: Water Resources Publications; 2000.

[7] Wardhana K, Hadipriono FC. Analysis of Recent Bridge Failures in the United States. J Perform Constr Facil 2003;17:144–51. https://doi.org/10.1061/(ASCE) 0887-3828(2003)17:3(144).

[8] MA, Khan, DP, McCrum, LJ, Prendergast, EJ, Obrien, PC,Fitzgerald, C-W, Kim Laboratory investigation of a bridge scour monitoring method using decentralized modal analysis. Struct Heal Monit 2021. doi:10.1177/1475921720985122.

[9] Forde MC, McCann DM, Clark MR, Broughton KJ, Fenning PJ, Brown A. Radar measurement of bridge scour. NDT&E Int 1999;32:481–92.

[10] Briaud JL, Ting F, Chen HC. SRICOS: prediction of Scour Rate in Cohesive Soils at Bridge Piers. J Geotech Geoenviron Eng 1999:237–46.

[11] Prendergast LJ, Gavin K. A review of bridge scour monitoring techniques. J Rock Mech Geotech Eng 2014;6:138–49. https://doi.org/10.1016/j.jrmge.2014.01.007.

[12] Heidarpour M, Afzalimehr H, Izadinia E. Reduction of local scour around bridge pier groups using collars. Int J Sediment Res 2010;25:411–22. https://doi.org/10.1016/S1001-6279(11)60008-5.

[13] A, Malekjafarian, LJ, Prendergast, EJ, OBrien Use of mode shape ratios for pier scour monitoring in two-span integral bridges under changing environmental conditions. Can J Civ Eng 2020;47:962–73. doi:10.1139/cjce-2018-0800.

[14] Malekjafarian A, Kim C, Obrien EJ, Prendergast LJ, Fitzgerald PC, Nakajima S. Experimental demonstration of a mode shape-based scour monitoring method for multi-span bridges with shallow foundations. J Bridg Eng 2020:25. https://doi.org/10.1061/(ASCE)BE.1943-5592.0001586.

[15] Prendergast LJ, Hester D, Gavin K. Determining the presence of scour around bridge foundations using vehicle-induced vibrations. J Bridg Eng 2016:21. https://doi.org/10.1061/(ASCE)BE.1943-5592.0000931.

[16] Xiong W, Kong B, Tang P, Ye J. Vibration-based identification for the presence of scouring of cable-stayed bridges. J Aerosp Eng 2018:31. https://doi.org/10.1061/(ASCE)AS.1943-5525.0000826.

[17] Bao T, Liu Z. Vibration-based bridge scour detection: A review. Struct Control Heal Monit; 2016.

[18] Prendergast LJ, Limongelli MP, Ademovic N, Anzlin A, Gavin KG, Zanini MA. Structural health monitoring for performance assessment of bridges under flooding and seismic actions. Struct Eng Int 2018;28:296–307.

[19] Lagasse PF, Zevenbergen LW, Clopper PE. Effects of debris on bridge pier scour. In: Burns SE, Bhatia SK, Avila CMC, Hunt BE, editors. Proc. 5th Int. Conf. Reston (VA), USA: Scour Eros; 2010. p. 854–63.

[20] Klinga JV, Alipour A. Assessment of structural integrity of bridges under extreme scour conditions. Eng Struct 2015;82:55–71. https://doi.org/10.1016/j.engstruct.2014.07.021.

[21] Tubaldi E, Macorini L, Izzuddin BA. Three-dimensional mesoscale modelling of multi-span masonry arch bridges subjected to scour. Eng Struct 2018;165:486–500. https://doi.org/10.1016/j.engstruct.2018.03.031.

[22] Foti S, Sabia D. Influence of foundation scour on the dynamic response of an existing bridge. J Bridg Eng 2011;16:295–304. https://doi.org/10.1061/(ASCE)BE.1943-5592.0000146.

[23] BE, Hunt NCHRP synthesis 396: Monitoring Scour Critical Bridges - A Synthesis of Highway Practice. Washington, DC: 2009.

[24] Briaud JL, Hurlebaus S, Chang K, Yao C, Sharma H, Yu O, et al. Realtime monitoring of bridge scour using remote monitoring technology, vol. 7. TX: Austin; 2011.

[25] Yu X. Time domain reflectometry automatic bridge scour measurement system: principles and potentials. Struct Heal Monit 2009;8:463–76. https://doi.org/10.1177/1475921709340965.

[26] M, Fisher, MN, Chowdhury, A a, Khan, S, Atamturktur An evaluation of scour measurement devices. Flow Meas Instrum 2013;33:55–67. doi:10.1016/j.flowmeasinst.2013.05.001.

[27] Nassif H, Ertekin AO, Davis J. Evaluation of bridge scour monitoring methods. NJ: Trenton; 2002.

[28] Anderson NL, Ismael AM, Thitimakorn T. Ground-penetrating radar : a tool for monitoring bridge scour. Environ Eng Geosci 2007.

[29] Zarafshan A, Iranmanesh A, Ansari F. Vibration-Based Method and Sensor for Monitoring of Bridge Scour. J Bridg Eng 2012;17:829–38. https://doi.org/10.1061/(ASCE)BE.1943-5592.0000362.

[30] De Falco F, Mele R. The monitoring of bridges for scour by sonar and sedimetri. NDT&E Int 2002;35:117–23.

[31] Prendergast LJ, Hester D, Gavin K, O'Sullivan JJ. An investigation of the changes in the natural frequency of a pile affected by scour. J Sound Vib 2013;332:6685–702. https://doi.org/10.1016/j.jsv.2013.08.020i.

[32] Prendergast LJ, Hester D, Gavin K. Development of a Vehicle-Bridge-Soil Dynamic Interaction Model for Scour Damage Modelling. Shock Vib 2016; 2016.. https://doi.org/10.1155/2016/7871089.

[33] Prendergast LJ, Gavin K, Hester D. Isolating the location of scour-induced stiffness loss in bridges using local modal behaviour. J Civ Struct Heal Monit 2017;7:483–503. https://doi.org/10.1007/s13349-017-0238-3.

[34] Kong X, Cai CS. Scour Effect on Bridge and Vehicle Responses under Bridge-Vehicle-Wave Interaction. J Bridg Eng 2016;21:1–16. https://doi.org/10.1061/(ASCE)BE.1943-5592.0000868.

[35] Ju SH. Determination of scoured bridge natural frequencies with soil–structure interaction. Soil Dyn Earthq Eng 2013;55:247–54. https://doi.org/10.1016/j.soildyn.2013.09.015.

[36] Chen C-C, Wu W-H, Shih F, Wang S-W. Scour evaluation for foundation of a cable-stayed bridge based on ambient vibration measurements of superstructure. NDT E Int 2014;66:16–27. https://doi.org/10.1016/j.ndteint.2014.04.005.

[37] Elsaid A, Seracino R. Rapid assessment of foundation scour using the dynamic features of bridge superstructure. Constr Build Mater 2014;50:42–9. https://doi.org/10.1016/j.conbuildmat.2013.08.079.

[38] Giordano PF, Prendergast LJ, Limongelli MP. A framework for assessing the value of information for health monitoring of scoured bridges. J Civ Struct Heal Monit 2020;10:485–96.

[39] Giordano, P.F., Prendergast, L.J., Limongelli, M.P., Quantifying the value of SHM information for bridges under flood-induced scour. Struct Infrastruct Eng 2022;(In Press).

[40] CEN. European standard EN 1993-1-1:2005. Eurodoce 3: Design of steel structures - Part 1-1: General rules and rules for buildings. Brussels: European Committee for Standardization; 2005.

[41] CEN. European standard EN 1992-1-1:2004. Eurocode 2: Design of concrete structures - Part 1-1: General rules and rules for buildings. Brussels: European Committee for Standardization; 2004.

[42] M, Kosič, A, Anžlin oVERFLOw Project Deliverable D4.2: Report on Vulnerability Assessment Methodology - Fragility curves for bridges subjected to flooding. Available from: https://projectoverflow.eu/public-documents/. 2022.

[43] Janbu N. Sediment deformations. University of Trondheim, Norwegian University of Science and Technology; 1998. p. 86. Bulletin 3,.

[44] Fellenius BH. Basics of Foundation Design Basics of Foundation Design. Electronic Edition (www.Fellenius.net); 2009.

[45] Kolarić D, Tusić Ž. Flood protection system of the city of karlovac – sensitivity of the input parameters. In: Biondić D, Holjević D, Vizner M, editors. 7th Croat. Water Conf. with Int. Partecip., Opatija, Croatia: Hrvatske vode; 2019. p. 723–32.

[46] M, Kosič, D, Hekič, J, Kalin, A, Anžlin oVERFLOw Project Deliverable 3.2: Report on investigation works and monitoring of bridges. Available from: https://projectoverflow.eu/public-documents/. 2021.

[47] M, Zhu The OpenSeesPy Library, Version 3.2.2 – 2020. 2020.

[48] McKenna F. OpenSees: A Framework for Earthquake Engineering Simulation. Comput Sci Eng 2011;13:58–66. https://doi.org/10.1109/MCSE.2011.66.

[49] CSI SAP2000 - Structural analysis and design software. Comput Struct Inc 2021.

[50] Kwon YW, Bang H. The finite element method using MATLAB. Boca Raton, FL: CRC Press, Inc.; 2000.

[51] Pais A, Kausel E. Approximate formulas for dynamic stiffnesses of rigid foundations. Soil Dyn Earthq Eng 1988;7:213–27. https://doi.org/10.1016/S0267-7261(88)80005-8.

[52] Gazetas G. Formulas and charts for impedances of surface and embedded foundations e. J Geotech Eng 1991:117.

[53] Gazetas G, Anastasopoulos I, Adamidis O, Kontoroupi T. Nonlinear rocking stiffness of foundations. Soil Dyn Earthq Eng 2013;47:83–91. https://doi.org/10.1016/j.soildyn.2012.12.011.

[54] Prendergast LJ, Igoe D. Examination of the reduction in natural frequency of laterally loaded piles due to strain-dependence of soil shear modulus. Ocean Eng 2022;258:111614. https://doi.org/10.1016/j.oceaneng.2022.111614.

[55] Van Impe WF, Wang S-T. The advanced p-y method for analyzing the behaviour of large-diameter monopiles supporting offshore wind turbines. E3S Web Conf 2020; 205:12008. https://doi.org/10.1051/e3sconf/202020512008.

[56] OpenSeesWiki - PySimple 1 Material n.d.

[57] OpenSeesWiki - TzSimple1 Material n.d.

[58] OpenSeesWiki - QzSimple 1 Material n.d.

[59] OpenSeesWiki - ElasticPP Material n.d.

[60] API. Recommended Practice for Planning, Designing and Constructing Fixed Offshore Platforms—Working Stress Design. Washington, D.C.: 2003.

[61] Reese LC, Van Impe WF. Single piles and pile groups under lateral loading -. 2nd Edition. 2nd Editio. CRC Press, Taylor & Francis Group; 2011.

[62] Burd HJ, Taborda DMG, Zdravković L, Abadie CN, Byrne BW, Houlsby GT, et al. PISA design model for monopiles for offshore wind turbines: application to a marine sand. Géotechnique 2020;70:1048–66. https://doi.org/10.1680/jgeot.18.P.277.

[63] Mosher R. Load-transfer criteria for numerical analysis of axially loaded piles in sand. Mississippi: Vicksburg; 1984.

[64] API. RP2A: Recommended practice for planning, designing and constructing offshore platforms - Working stress design. Washington, DC: 2007.

[65] VN, Vijayvergiya Load-movement characteristics of piles. 4th Annu. Symp. Waterw. Port, Coastal, Ocean Div., Los Angeles, US: ASCE; 1977, p. 1256–66.

[66] Meyerhof GG. Some recent research on the bearing capacity of foundations. Can Geotech J 1963;1:16–26. https://doi.org/10.1139/t63-003.

[67] Burland JB, Burbidge MC. Settlement of foundations on sand and gravel. Proc Inst Civ Eng 1985;78:1325–81. https://doi.org/10.1680/iicep.1985.1058.

[68] Standards Australia. Australian standard AS-5100.2-2004. Bridge desing - Part 2: Design loads. Sydney, Australia: 2004.

[69] LA, Arneson, LW, Zevenbergen, PF, Lagasse, PE, Clopper Evaluating Scour at Bridges. Fifth Edition, Hydraulic Engineering Circular No. 18. US Dep Transp Fed Highw Adm 2012.

[70] Tubaldi E, White CJ, Patelli E, Mitoulis SA, De Almeida G, Brown J, et al. Invited perspectives: challenges and future directions in improving bridge flood resilience. Nat Hazards Earth Syst Sci 2022;22:795–812. https://doi.org/10.5194/nhess-22-795-2022.

[71] Li Q, Prendergast LJ, Askarinejad A, Chortis G, Gavin K. Centrifuge modeling of the impact of local and global scour erosion on the monotonic lateral response of a monopile in sand. Geotech Test J 2020:43. https://doi.org/10.1520/GTJ20180322.

[72] Chortis G, Askarinejad A, Prendergast LJ, Li Q, Gavin K. Influence of scour depth and type on p–y curves for monopiles in sand under monotonic lateral loading in a geotechnical centrifuge. Ocean Eng 2020;197:106838. https://doi.org/10.1016/j.oceaneng.2019.106838.

[73] Qi W, Gao F, Randolph M, Lehane B. Scour effects on p–y curves for shallowly embedded piles in sand. Géotechnique 2016.

[74] Kariyawasam KD, Middleton CR, Madabhushi G, Haigh SK, Talbot JP. Assessment of bridge natural frequency as an indicator of scour using centrifuge modelling. J Civ Struct Heal Monit 2020;10:861–81. https://doi.org/10.1007/s13349-020-00420-5.

[75] Ahamed T, Duan JG, Jo H. Flood-fragility analysis of instream bridges–consideration of flow hydraulics, geotechnical uncertainties, and variable scour depth. Struct Infrastruct Eng 2021;17:1494–507. https://doi.org/10.1080/15732479.2020.1815226.

[76] Hung C-C, Yau W-G. Vulnerability evaluation of scoured bridges under floods. Eng Struct 2017;132:288–99. https://doi.org/10.1016/j.engstruct.2016.11.044.

[77] Ko Y-Y, Chiou J-S, Tsai Y-C, Chen C-H, Wang H, Wang C-Y. Evaluation of flood-resistant capacity of scoured bridges. J Perform Constr Facil 2014;28:61–75. https://doi.org/10.1061/(asce)cf.1943-5509.0000381.

[78] Bao T, Andrew Swartz R, Vitton S, Sun Y, Zhang C, Liu Z. Critical insights for advanced bridge scour detection using the natural frequency. J Sound Vib 2017; 386:116–33. https://doi.org/10.1016/j.jsv.2016.06.039.